Rac GTPase activating protein ARHGAP25 regulates leukocyte transendothelial migration in mice

Running title: ARHGAP25 regulates leukocyte migration

Roland Csépányi-Kömi[*,†,#], Éva Wisniewski[*,#], Balázs Bartos[*], Petra Lévai[*], Tamás Németh[*], Bernadett Balázs[*], Angela R. M. Kurz[†], Susanne Bierschenk[†], Markus Sperandio[†,§], Erzsébet Ligeti[*,§]

[*] Department of Physiology, Semmelweis University, Budapest, Hungary

[†] Walter Brendel Center of Experimental Medicine, Ludwig-Maximilians Universität, Munich, Germany

[#, §] these authors contributed equally

Corresponding author: Professor Erzsébet Ligeti

Department of Physiology, Semmelweis University

1094 Budapest, Tűzoltó u. 37-47., Hungary

Phone: +361 459 1500 ext. 60457; Fax: +361 266 7480

Email: ligeti.erzsebet@med.semmelweis-univ.hu

Abstract

ARHGAP25 is a Rac-specific GTPase activating protein that is expressed primarily in hematopoietic cells. The involvement of ARHGAP25 in regulating the recruitment of leukocytes to inflammatory sites was investigated in genetically modified mice. Using intravital microscopy we show that *Arhgap25*-deficiency affects all steps of leukocyte recruitment with a predominant enhancement of transendothelial migration of neutrophilic granulocytes. Increased transmigration of *Arhgap25*-deficient leukocytes is demonstrated in inflamed cremaster muscle venules, in a peritonitis model, and in an *in vitro* chemotaxis assay. Using bone marrow chimeric mice lacking ARHGAP25 in the hematopoietic compartment, we show that enhanced migration in the absence of ARHGAP25 is due to defective leukocyte function. In search for potential mechanisms of ARHGAP25-regulated migration of neutrophils, we detected an increase in the amount of active, GTP-bound Rac and Rac-dependent cytoskeletal changes in the absence of ARHGAP25 suggesting a critical role of ARHGAP25 in counterbalancing the Rac-activating effect of nucleotide exchange factors. Taken together, using *Arhgap25*-deficient mice we identified ARHGAP25 as a relevant negative regulator of leukocyte transendothelial migration.

Introduction

In inflammation, neutrophil recruitment to sites of injury is essential for the fast and effective elimination of injurious agents. The first step of recruitment consists in the activation of vascular endothelial cells, which leads to increased expression of several cell surface molecules including selectins and integrin ligands (1, 2). These molecules are recognized by circulating leukocytes enabling the stepwise recruitment and extravasation of leukocytes into inflamed tissue. Capture to the inflamed endothelium is followed by rolling of leukocytes along the endothelium. Both capture and rolling are mediated by endothelial selectins and leukocyte expressed selectin ligands (3). During rolling, leukocytes get into intimate contact with the endothelial surface which enables binding of endothelium-expressed chemokines to their respective ligand on the leukocyte surface triggering firm arrest of leukocyte on the endothelium. Thereafter, leukocytes begin to crawl along the vessel wall searching for an appropriate exit point for transmigration into tissue (diapedesis) (2, 4, 5). Extravasated leukocytes are directed by chemotactic agents to the pathogens to be eliminated (6). All these different types of movements require a precise spatial and temporal organization of the actin cytoskeleton (7-9). Although our knowledge on the involved receptors and signaling pathways has increased tremendously in the last decade (10), differences in the molecular organization of the actin cytoskeleton underlying the different types of movements are still poorly understood.

Members of the Rac/Rho subfamily of small GTP-binding proteins are key regulators of the actin cytoskeleton (11). Their prevalence in the active, GTP-bound state depends on the balance between the three major regulatory proteins: guanine nucleotide exchange factors (GEFs) that promote the active state, GTPase activating proteins (GAPs) that counteract it, and guanine nucleotide dissociation inhibitors (GDI) that conserve the inactive state (12, 13). In case of the Rac/Rho subfamily, the potential number of GEFs and GAPs expressed in a

specific cell is especially high (14). The majority of these GEFs and GAPs are large proteins composed of several effector, interactive and regulatory domains that suggest multiple functions (13, 14). In neutrophils, a specific involvement of certain GEFs has been investigated for different neutrophil effector functions including chemotaxis and adhesion (15-17). In contrast, similar data on potentially interacting GAPs are still scarce (18-20).

In a recent study, we have shown that ARHGAP25 is a Rac-specific GAP expressed primarily in hematopoietic cells (21). We also demonstrated that ARHGAP25 serves as a negative regulator of phagocytosis and related superoxide production (21, 22). The aim of the present study was to reveal the role of ARHGAP25 in the complex process of leukocyte recruitment during inflammation. We provide the first detailed description of the *Arhgap25*$^{-/-}$ mice, and show that loss of ARHGAP25 affects several steps along the recruitment cascade leading to a proinflammatory phenotype with elevated transmigration of neutrophils into inflamed tissue which is accompanied by increased Rac activity in neutrophils.

Materials and Methods

Antibodies and reagents

Anti-CD11b-PE and anti-Ly-6G-Pacific Blue were purchased from BioLegend, rat IgG2bκ-PE isotype control and anti-CD18-FITC from BD Biosciences, rat IgG2a-APC isotype control, anti-CD11a-APC, anti-human Fcγ-biotin, Streptavidin-PECy5 and rat IgG2a-FITC isotype control from eBioscience, anti-CXCR2-APC, recombinant murine (rm) TNFα, rmE-selectin/CD62E-Fc chimera and rmICAM-1/CD54-Fc chimera from R&D Systems, rmKC/CXCL-1 and rmCXCL12 from PreproTech, Ly-6G-PerCP-Cy5.5 and CD11b-PE from BD Pharmingen, mouse anti-Rac antibody from BD Transduction Laboratories, paraformaldehyde from Sigma-Aldrich. Anti-human ARHGAP25 polyclonal antibody was prepared as described previously.(21) Cross-reactivity with mouse ARHGAP25 was tested using the lysate of COS-7 cells transfected with human *ARHGAP25-V5* and mouse *Arhgap25-V5* constructs (see Fig. S1 for details). All other reagents were of research grade.

Mice

The *Arhgap25*$^{-/-}$ mouse strain used for this research project was created from ES cell clone (EPD0085_1_C10) obtained from the NCRR-NIH supported KOMP Repository (www.komp.org) and generated by the CSD consortium for the NIH funded Knockout Mouse Project (KOMP). Methods used on the CSD targeted alleles have been published in (23). *Arhgap25*$^{-/-}$ mice had a C57BL/6 genetic background and were maintained in a homozygous breeding colony. Genotyping was performed according to KOMP's instructions using the following primers: Common-loxP-F: 5'-GAGATGGCGCAACGCAATTAAT-3'; CSD-Arhgap25-SR1: 5'- GCATGAGGCAGCTGTTCTTAGTTACC-3'; CSD-Arhgap25-GF4: 5'-TGCACACGGTGGCATCTCTACTAAAG-3'. Analysis of blood parameters was carried out with a haemocytometer. To reveal differences in body weight between wild type and

Arhgap25$^{-/-}$ mice, 5-week-old animals (3 males/genotype and 2 females/genotype) were weighed for 14 weeks. *Arhgap25*$^{-/-}$ and control wild-type bone marrow chimeras were generated using bone marrow cells from adult donors as described previously (24, 25). *Arhgap25*$^{-/-}$ bone marrow cell suspensions were injected intravenously into lethally irradiated (11.5-Gy) recipients carrying the CD45.1 allele on the C57BL/6 genetic background. An equal number of control chimeras were also generated using *Arhgap25*-expressing (*Arhgap25*$^{+/+}$) bone marrow cells and will be referred to as wild-type chimeras. Efficiency of repopulation of the hematopoietic compartment by donor-derived cells was more than 98%, tested 4 weeks after transplantation by flow cytometry: we tested the expression of CD45.2 (donor) allele in the granulocyte gate determined by Ly-6G-staining, as described previously (24, 25) (data not shown). Bone marrow chimeras were used 4-8 weeks after transplantation. Mouse strain carrying the CD45.1 allele on the C57BL/6 genetic background (B6.SJL-Ptprca) was purchased from The Jackson Laboratory (Bar Harbor, ME). Mice were kept in individually sterile ventilated cages (Tecniplast, Buguggiate, Italy) in a conventional facility. Age and gender-matched animals were used for all the experiments. Animal experiments were approved by the Regierung von Oberbayern, Germany, AZ 55.2.1.54-2532-76-12, and by the Governmental Office of Pest County, Hungary (22.1/S321/3/2011).

Intravital microscopy of the mouse cremaster muscle

Mice were pretreated with intrascrotal injection of 500 ng rmTNFα per mice. After 2 h, mice were anesthetized and trachea and carotid artery were cannulated. Scrotum was opened, the cremaster muscle exteriorized, spread over a cover glass and superfused with 35 °C bicarbonate-buffered saline as described (26). Parameters of rolling, adhesion and crawling were determined using an Olympus BX51WI intravital microscope equipped with a saline immersion objective (40/0.8 NA, Olympus) and a CCD camera (model CF8/1, Kappa). All

scenes were recorded by the Virtual Dub software for later offline analysis. Systemic blood samples (~ 50 µL) were collected through the carotid artery catheter before and during the experiment and analysed using a haemocytometer. The offline analysis of venular diameter and vessel segment length of postcapillary venules (between 20-40 µm in diameter) was carried out with Fiji software (27). Leukocyte rolling flux fraction was calculated from the number of rolling cells that crossed a perpendicular line through a given vessel within 1 min in relation to the total number of circulating leukocytes (28). Velocities of rolling and crawling were measured using MTrackJ plugin of Fiji software. Other experimental parameters (centerline blood flow velocity, shear rate, systemic cell counts) are shown in Table SI.

TNFα-induced peritonitis model

Mice were treated with intraperitoneal injection of 5 µg rmTNFα in a final volume of 100 µL. Three hours after treatment, mice were sacrificed and peritoneal cavity was washed with 5 mL ice-cold PBS supplemented with 20 mM HEPES and 10 mM EDTA. Ly-6G^{+} infiltrated cells were analysed with BD FACSCalibur device. Cell counts were determined using Flow-Count Fluorospheres (Beckman Coulter).

Histology

Three hours after intrascrotal injection of rmTNFα (500 ng in 200 µL/mouse) or sterile PBS (200 µL/mouse), cremaster muscles were exteriorized, mounted on adhesive slides (Superfrost, Thermo Scientific) and fixed in 4% (w/v) paraformaldehyde for at least 48 h at 4°C. Then samples were washed 3x5 min in 0.1 M Phosphate buffer (0.1 M NaH_2PO_4, 0.1 M Na_2HPO_4 mixed in 81:19 ratio, pH 7.4) supplemented with 5% (v/v) ethanol and stained with Giemsa's azure eosin methylene blue solution (Merck) for 4 min. After a rinse with water,

slices were differentiated with 0.03% (v/v) acetic acid for 10 min, and immersed in ascending alcohol series from 70% (v/v) to absolute alcohol, in each for 3 min. Draining was carried out with xylol (2x5 min), followed by sealing with rectangular coverslips using Eukitt (Sigma-Aldrich). Whole mounts were analyzed with a Zeiss microscope equipped with an oil immersion objective (100x/1.4 NA, Zeiss). Whole mounts of bone marrow chimeras were analyzed with a Leica DMI 6000 B microscope equipped with an oil immersion objective (63x/1.25 NA, Leica).

After 3 hours of TNFα challenge peritoneal tissue samples were taken and fixed in 4% (w/v) phosphate-buffered paraformaldehyde for 48 hours. The tissue samples were paraffin-processed, embedded, and 4 µm sections cut with a Microm HM340E rotary microtome (Thermo Fisher Scientific). Cut sections were then used for hematoxylin and eosin (H&E) staining. Representative pictures were captured with a Nikon ECLIPSE N*i* microscope equipped with 10x/0.30 NA and 40x/0.75 NA dry objectives (Nikon) and a Nikon DS-Ri2 camera. Images were processed with NIS Elements v4.50 Imaging Software (Nikon).

Ex vivo flow chamber assay

Glass capillaries (Rectangular Boro Capillaries, 0.04x0.40mm, VitroCom) were coated overnight with rmE-selectin (CD62E Fc chimera, 20 µg/mL) or a combination of rmE-selectin and rmICAM-1 (ICAM-1 Fc chimera, 15 µg/mL) or a combination of rmE-selectin and rmICAM-1 and rmKC/CXCL-1 (15 µg/mL) at 4°C followed by blocking with 5% (w/v) casein (Sigma-Aldrich) in PBS for 2h. Carotid artery catheter was connected directly to one end of the chamber; while the other end was left open to regulate blood flow (shear stress level was at 3-4 dyn/cm^2). One representative field was recorded for 5 min using an Olympus BX51WI intravital microscope equipped with a water immersion objective (40/0.8 NA,

Olympus) and a CCD camera (model CF8/1, Kappa). Rolling velocity was determined using MTrackJ plugin of Fiji software.

Transwell migration assay

In vitro migration of neutrophils was tested using a Transwell (Corning) assay with inserts of 3 µm pore size coated with 10% fetal bovine serum (FBS) for 1 hour at 37°C. Isolated cells were pretreated with 50 µg/mL TNFα for 10 min in a 37°C incubator humidified with 5% CO_2. For chemoattractant, 50ng/mL CXCL12 was used per well, containing $1x10^6$ cells. After 1 hour incubation at 37°C, transmigrated cells were counted using an acid phosphatase assay (29).

Determination of leukocyte adhesion proteins and filamentous actin

Neutrophils were isolated from bone marrow with percoll gradient centrifugation as described previously (30). To determine cell surface expression of several receptors involved in neutrophil migration, 100 µL whole blood was obtained retro-orbitally from wild type and knock out mice pretreated with 500 ng TNFα intrascrotally for 2 h. Alternatively, transmigrated cells were collected from the Transwell plate. Then, whole blood or transmigrated neutrophil samples were transferred into 5 mL centrifuge tubes. Samples were washed once with 3 mL $HBSS^+$ medium (Hank's Balanced Salt Solution (Sigma-Aldrich) supplemented with 1 mM $CaCl_2$, 1 mM $MgCl_2$, 0.1% (w/v) glucose, 10 mM HEPES and 0.25% (w/v) Bovine Serum Albumin (BSA), pH 7.4) and centrifuged with 350g for 5 min at RT. Cells were stained with the indicated antibodies diluted in FACS buffer (PBS containing 1% (w/v) BSA), for 20 min at 4°C. After staining, 1 mL FACS Lysing Solution (BD BioSciences) was added to the samples and cells were fixed on ice for 10 min. Then cells were centrifuged with 350 g for 5 min at RT, resuspended in 300 µL FACS buffer and

analyzed by flow cytometry (Beckman Coulter Gallios). For actin-staining, $1x10^6$ bone marrow derived neutrophils were fixed with 4% (w/v) paraformaldehyde for 20 min at RT and centrifuged with 500 g for 5 min at RT. Cells were permeabilized with 0.1% (v/v) Triton-X-100 for 5 min at RT, then stained with Alexa-488-phalloidin (Life Technologies) in 1:500 dilution for 20 min at RT. Filamentous actin amount was analyzed with BD FACSCalibur device. To investigate actin-polymerization in time, $1x10^6$ bone marrow derived neutrophils were stimulated with 50 ng/mL TNFα from 0 to 15 min at 37 °C. After stimulation, cells were fixed and labelled with Alexa-488-phalloidin as detailed above.

Soluble ICAM-1 binding assay

For each sample, $1.5x10^6$ cells were resuspended in 30 µl $HBSS^+$ and prewarmed at 37°C for 1 min. Pre-complexed master mix containing rmICAM-1-human Fc in 20 µg/mL, anti-human IgG1-biotin in 10 µg/mL, Streptavidin-PE-Cy5 in 1:100 dilution and the indicated stimulus were also prewarmed for 10 min at 37°C. Then, 10 µL pre-complexed master mix was added to 30 µL cell suspension and incubated for 3 min at 37°C. Reaction was stopped with 900 µL ice-cold FACS Lysing Solution, samples were transferred on ice and fixed for 10 min. Cells were washed with 2 mL $HBSS^+$ and centrifuged with 350 g for 5 min at 4 °C. Then cells were stained with anti-Ly-6G-Pacific Blue in 1:600 dilutions for 20 min at 4°C. After a washing step (350 g, 5 min at 4°C in 2 mL $HBSS^+$), cells were resuspended in 300 µL $HBSS^+$ and analyzed by flow cytometry (Beckman CoulterGallios).

Measurement of the amount of active Rac

The cellular levels of GTP loaded Rac were determined with pull-down assay using GST fusion proteins containing the GTPase-binding domain of p21-activated kinase (PAK) (GST-PBD) as described (31, 32). GST-PBD has been expressed in *Escherichia coli*. For pull-down,

bone marrow-derived neutrophils were activated with 50 ng/mL TNFα in $HBSS^{+}$ medium at 37 °C for 10 min. Basal Rac-activation was determined from resting cells. Whole cell lysates were run on SDS-PAGE, blotted onto nitrocellulose (33) and stained with anti-Rac antibody in 1:5000 dilution. Bound antibody was detected with enhanced chemiluminescence using horseradish peroxidase-conjugated anti–mouse-Ig (from sheep) secondary antibody (GE Healthcare) used in 1:5000 dilution. ImageJ software was used for densitometry analysis.

Statistical analysis

All data were analyzed and plotted using SigmaPlot 11.0 Software (Systat Software, Inc.). Pairwise comparison of experimental groups was carried out with paired t-test or Mann-Whitney Rank Sum Test or two way ANOVA followed by a Tukey post-hock test, depending on the condition. All *P*-values<.05 were considered statistically significant.

Results

Arhgap25 knockout mice

Arhgap25 knockout mice were generated by the CSD consortium for the NIH funded Knockout Mouse Project (KOMP) inserting the L1L2_Bact_P cassette upstream of the 6th exon of the *Arhgap25* gene. The cassette contains the following sites and sequences in the given order: FRT, lacZ, loxP, neomycin (under the control of the human beta-actin promoter), SV40 polyA, FRT, loxP. A third loxP site was inserted downstream of the 6th exon (23). Fertile homozygous mice (*Arhgap25*$^{-/-}$) were obtained with the expected Mendelian ratios (data not shown) and did not show any obvious phenotype. No ARHGAP25 protein could be detected in either bone marrow derived neutrophils or in the spleen of *Arhgap25*$^{-/-}$ mice (Fig. S1A, B). Blood panel (e.g. circulating cell counts, hematocrit, mean corpuscular hemoglobin, mean corpuscular hemoglobin concentration) of *Arhgap25*$^{-/-}$ mice did not differ from the wild type (*Arhgap25*$^{+/+}$) (Table I, Table SII). We assessed the body weight of male and female mice during a 130 days period and in 3 independent experiments. Body weight of male *Arhgap25*$^{-/-}$ mice was decreased compared to wild type but in the case of female mice, no difference was observed (Fig. S2).

Reduced leukocyte rolling velocity and prolonged crawling in the absence of ARHGAP25

Using intravital microscopy, we first investigated leukocyte rolling, adhesion and crawling in TNFα-stimulated cremaster muscle venules of WT (*Arhgap25*$^{+/+}$) and *Arhgap25*$^{-/-}$ mice *in vivo*. Microvessel diameters, wall shear rates, centerline blood flow velocities and circulating leukocyte counts were similar between wild type and *Arhgap25*$^{-/-}$ mice (Table SI). While we observed no difference in leukocyte rolling (Fig. 1A), mean leukocyte rolling velocity was

markedly decreased in the absence of ARHGAP25 (Fig. 1B). Furthermore, we analyzed the number of adherent leukocytes and found no difference in adhesion between *Arhgap25*$^{-/-}$ and WT mice (Fig. 1C). Next, we investigated leukocyte crawling along the inflamed endothelium. Individual crawling paths of >140 cells were analyzed per group (Fig. 1D and E). We did not observe any difference in crawling directionality or accumulated distance between WT and ARHGAP25$^{-/-}$mice (Fig. 1D-F). However, we found a significant increase in crawling velocity and Euclidean distance in *Arhgap25*$^{-/-}$ mice compared to WT mice (Fig. 1G and H) suggesting that ARHGAP25 is regulating leukocyte crawling *in vivo*.

Lack of ARHGAP25 augments transendothelial migration *in vivo*.

Next, we studied leukocyte extravasation in TNFα-stimulated cremaster muscle whole mount preparations of WT and *Arhgap25*$^{-/-}$ mice. As shown in Fig. 2A-B, *Arhgap25*$^{+/+}$ leukocytes were found mainly in the vessels and the extravasated cells were scattered in the tissue. In contrast, a large number of *Arhgap25*$^{-/-}$ leukocytes lined up around the vessel from which they extravasated (Fig. 2C-D). Transendothelial migration was quantified and we found a significant increase in leukocyte extravasation in *Arhgap25*$^{-/-}$ compared to WT mice (Fig. 2E). Intrascrotal injection of PBS as a control caused no significant difference between WT and *Arhgap25*$^{-/-}$ mice (P= 0.194, data not shown). Further analysis of the different leukocyte populations extravasated into the inflamed cremaster muscle tissue revealed that the major component of extravasated leukocytes were neutrophilic granulocytes (PMN), followed by monocytes and lymphocytes (marked as “Others”) and eosinophils (Fig. 2F). Increased leukocyte extravasation upon TNFα stimulus was confirmed in an acute peritonitis model. Analyzing the H&E stained sections of inflamed peritoneal tissue, elevated leukocyte infiltration was observed in *Arhgap25*$^{-/-}$ mice compared to WT (Fig. 3A). Specific analysis of

Ly-6G^{+} neutrophil count in peritoneal lavage revealed a significant increase in case of *Arhgap25*$^{-/-}$ neutrophils compared to WT (Fig. 3B).

Leukocyte rolling and adhesion under *ex vivo* conditions and *in vitro* Transwell migration assay.

As *Arhgap25*$^{-/-}$ mice are complete knockout mice, the question arose, whether the observed alterations are due to functional changes in leukocytes or endothelial cells. To investigate the contribution of leukocytes on the recruitment phenotype observed in *Arhgap25*$^{-/-}$ mice, we performed *ex vivo* flow chamber assays and assessed rolling and adhesion of leukocytes in flow chambers coated with adhesion relevant proteins. In flow chambers coated with recombinant murine (rm)E-selectin, we saw a 2.5-fold increase in the number of rolling *Arhgap25*$^{-/-}$ leukocytes compared to wild type leukocytes (Fig. 4A). Next, we analyzed leukocyte adhesion in flow chambers coated with rmE-selectin alone, with rmE-selectin and rmICAM-1, and with rmE-selectin, rmICAM-1 and rmCXCL-1. Similar to the *in vivo* results we found no difference in the number of adherent cells between the different groups (Fig. 4B). However, when we analyzed leukocyte rolling velocities, lack of ARHGAP25 resulted in a significant decrease in rolling velocity (Fig. 4C) in flow chambers coated with rmE-selectin or with rmE-selectin and rmICAM-1 surface (Fig. 4C).

Taken together, we were able to reproduce under *ex vivo* conditions the pattern of rolling and adherence observed in ARHGAP25-deficient animals under *in vivo* conditions suggesting that loss of ARHGAP25 in leukocytes accounts for the observed pro-inflammatory phenotype.

In order to test the role of ARHGAP25 in cell migration under *in vitro* conditions, we determined neutrophil migration toward CXCL12 in a Transwell assay. As shown in Fig. 4D,

313 *Arhgap25*$^{-/-}$ neutrophils pretreated with TNFα for 10 min showed a significant increase in
314 transmigration compared to WT.
315
316 **Verification of altered leukocyte function in bone marrow chimeras**
317 In view of the decisive role of the adhesive surface provided *in vivo* by the endothelial cells
318 we wanted to verify our flow chamber data in bone marrow chimeric mice. These animals
319 express the CD45.1 allele and carry *Arhgap25*$^{-/-}$ or *Arhgap25*$^{+/+}$ hematopoietic cell
320 populations that express CD45.2. Using these animals, we investigated the extravasation of
321 leukocytes in cremaster muscle whole mounts after 3 h local stimulation with TNFα. CD45.2-
322 expressing *Arhgap25*$^{-/-}$ leukocytes were able to transmigrate more efficiently in CD45.1-
323 expressing WT recipients than *Arhgap25*$^{+/+}$ cells (Fig. 5A-D). Similar to the results presented
324 in Fig. 2, we found a threefold increase in leukocyte extravasation in chimeric mice with
325 *Arhgap25*$^{-/-}$ hematopoietic cells compared to chimeric mice where WT hematopoietic cells
326 had been transferred (Fig. 5E). Similar to the results obtained in complete knock-out animals,
327 mainly neutrophilic granulocytes were responsible for the increase in extravasation followed
328 by mononuclear cells (marked as "Others") and eosinophils (Fig. 5F).
329 These results substantiate that the alteration of leukocyte transendothelial migration
330 observed in the absence of ARHGAP25 is due to primary changes in the hematopoietic
331 compartment but not in endothelial or other non-hematopoietic cell compartment.
332
333 **Potential mechanism of altered leukocyte function**
334 To examine, whether ARHGAP25 has a regulatory role in the expression of adhesion relevant
335 molecules and signaling events during neutrophil recruitment, we investigated cell surface
336 expression and ligand binding ability of receptors and molecules involved in leukocyte-
337 endothelial cell interactions. As shown in Fig. 6A, ARHGAP25 deficiency did not affect the

338 expression of β2 integrins (CD18, CD11a and CD11b), L-selectin (CD62L), PSGL-1,
339 chemokine receptor CXCR2 or CD44. *In vitro* analysis of adhesion molecule expression after
340 direct chemotactic migration of neutrophils did not reveal any difference between WT and
341 *Arhgap25*$^{-/-}$ cells either (data not shown). Lack of ARHGAP25 also did not result in any
342 difference in rmICAM-1 binding to LFA-1 in resting cells. As stimulation of bone marrow-
343 derived neutrophils leads to integrin activation and increased ligand binding (34), we also
344 investigated binding of rmICAM-1 to neutrophils stimulated with CXCL1 or PMA.
345 Compared to unstimulated controls, PMA caused a significant increase in rmICAM-1 binding
346 to LFA-1 on both *Arhgap25*$^{-/-}$ and wild type neutrophils. However, ARHGAP25-deficiency
347 did not influence rmICAM-1 binding to stimulated neutrophils. (Fig. 6B).

348 Our previous study indicated that ARHGAP25 has a regulatory role in neutrophilic
349 functions through its GAP activity on Rac1 (21). In addition, our *in vitro* studies demonstrate
350 that it has a GAP activity on Rac2 as well (data not shown). Therefore, we investigated the
351 presence of active Rac in bone marrow-derived neutrophils. Interestingly, we observed no
352 difference in Rac-activity between ARHGAP25$^{-/-}$ and wild type cells in the resting state (Fig.
353 6C). In contrast, treatment of neutrophils with TNFα resulted in a marked decrease of active
354 Rac in the presence of ARHGAP25, while the lack of ARHGAP25 completely abolished this
355 alteration (Fig. 6C).

356 As Rac is known to be a key regulator of actin-polymerization during leukocyte
357 migration (35, 36), we measured filamentous actin (F-actin) in *Arhgap25*$^{-/-}$ and wild type BM
358 neutrophils. In resting ARHGAP25-deficient cells, increased F-actin was observed compared
359 to wild type cells (Fig. 6D). Similar difference could be revealed upon stimulation with TNFα
360 (Fig. 6E). Taken together, we suggest that ARHGAP25 affects actin-polymerization and
361 depolymerization through its GTPase activating effect on Rac.

Discussion

The present study provides a detailed characterization of leukocyte recruitment during inflammation *in vivo* in ARHGAP25-deficient mice. Alterations have been uncovered for several steps along the recruitment cascade, indicating a role for the protein in those processes. Most remarkable is the increase of transmigrating neutrophils observed both in the inflamed cremaster muscle and the inflamed peritoneal cavity. No striking changes were found in circulating leukocyte counts between wild type and *Arhgap25*$^{-/-}$ animals excluding differences in circulating leukocyte numbers for the observed alterations in leukocyte recruitment in the absence of ARHGAP25.

Alteration of leukocyte migration may be the result of primary changes in circulating leukocytes, the endothelial cells, or both. Based on the following observations, we believe that in case of ARHGAP25-deficient animals, the altered migration is caused by leukocytes: i) ARHGAP25 was shown to be expressed primarily in hematopoietic cells (21) ii) all the trafficking alterations observed in living animals could be reproduced with isolated cells under *ex vivo* or *in vitro* condition iii) the difference between the movements of *Arhgap25*$^{+/+}$ and *Arhgap25*$^{-/-}$ cells was reproduced in bone marrow chimeric animals *in vivo*, where the deficiency affected only the hematopoietic but not the endothelial or other peripheral cells.

In control experiments it was verified that ARHGAP25-deficiency had no influence on the expression of the major leukocyte adhesive proteins and receptors or ligand binding of β2 integrins. On the other hand, stimulation of neutrophils with TNFα resulted in a significant decrease in measurable GTP-bound Rac which was abolished by absence of ARHGAP25. The observed increase in the amount of filamentous actin indicates the biological relevance of enhanced Rac activity (Fig. 6). Deficiency in various RacGEFs was reported to result in decreased amount of GTP-bound Rac and a decrease in phagocyte migration (16, 37, 38), i.e. changes opposite to our findings in animals lacking ARHGAP25. We thus ascribe the

alteration of leukocyte trafficking in ARHGAP25-deficient animals to cytoskeletal reorganization due to elevation of RacGTP concentration. In human endothelial cells (HUVECs), TNFα was shown to induce actin-rearrangement through activation of Rho family small G-proteins (39) and several studies reported the role of TNFα in neutrophil priming and its involvement in neutrophil effector functions and inside-out signaling (40-43). Our findings strongly suggest that the leukocyte-specific RacGAP ARHGAP25 is a critical player in TNFα-induced, Rac-mediated actin reorganization in neutrophils. Two recent reports provide important information on its physiological role: ARHGAP25 was shown to be required for actin depolymerization in the course of phagocytosis (21, 44), and it was demonstrated to undergo significant changes in its phosphorylation pattern and GAP activity upon biological stimulation (45). TNFα-initiated modulation of the phosphorylation pattern of ARHGAP25 with subsequent alterations of its GAP function may provide the link between the cytokine effect and the actin cytoskeleton rearrangement.

Taken together, our data indicate that ARHGAP25 is a critical negative regulator of Rac activity and leukocyte transmigration. This qualifies ARHGAP25 as an interesting drug target in autoimmune disorders (e.g. rheumatoid arthritis and multiple sclerosis) where leukocyte recruitment is unwanted.

Acknowledgements

The authors are indebted to Professor Attila Mócsai for helpful suggestions and critical reading of the manuscript and to Ms. Regina Tóth-Kun and Nadine Schmidt for expert technical assistance.

Authorship contributions

R. Csépányi-Kömi and É. Wisniewski carried out the majority of experiments and prepared writing of the manuscript; B. Bartos, P. Lévai, A. Kurz and S. Bierschenk carried out part of the experiments; T. Németh carried out the bone marrow transplantation; B. Balázs carried out the histology on murine peritoneums; M. Sperandio and E. Ligeti supervised, coordinated and financed the experimental work and had a major role in writing of the manuscript.

Disclosure of Conflict of Interest

The authors have no conflict of interest to disclose.

References

1. Rao, R. M., L. Yang, G. Garcia-Cardena, and F. W. Luscinskas. 2007. Endothelial-dependent mechanisms of leukocyte recruitment to the vascular wall. *Circ Res* 101: 234-247.
2. Ley, K., C. Laudanna, M. I. Cybulsky, and S. Nourshargh. 2007. Getting to the site of inflammation: the leukocyte adhesion cascade updated. *Nat Rev Immunol* 7: 678-689.
3. McEver, R. P. 2002. Selectins: lectins that initiate cell adhesion under flow. *Curr Opin Cell Biol* 14: 581-586.
4. Luster, A. D., R. Alon, and U. H. von Andrian. 2005. Immune cell migration in inflammation: present and future therapeutic targets. *Nat Immunol* 6: 1182-1190.
5. Zarbock, A., and K. Ley. 2009. Neutrophil adhesion and activation under flow. *Microcirculation* 16: 31-42.
6. Borregaard, N. 2010. Neutrophils, from marrow to microbes. *Immunity* 33: 657-670.
7. Insall, R. H., and L. M. Machesky. 2009. Actin dynamics at the leading edge: from simple machinery to complex networks. *Dev Cell* 17: 310-322.
8. Meyer, W. H., and T. H. Howard. 1987. Actin polymerization and its relationship to locomotion and chemokinetic response in maturing human promyelocytic leukemia cells. *Blood* 70: 363-367.
9. Vicente-Manzanares, M., and F. Sanchez-Madrid. 2004. Role of the cytoskeleton during leukocyte responses. *Nat Rev Immunol* 4: 110-122.
10. Futosi, K., S. Fodor, and A. Mocsai. 2013. Neutrophil cell surface receptors and their intracellular signal transduction pathways. *Int Immunopharmacol* 17: 638-650.
11. Hall, A. 1998. Rho GTPases and the actin cytoskeleton. *Science* 279: 509-514.
12. Csepanyi-Komi, R., M. Levay, and E. Ligeti. 2012. Rho/RacGAPs: embarras de richesse? *Small GTPases* 3: 178-182.
13. Ligeti, E., S. Welti, and K. Scheffzek. 2012. Inhibition and termination of physiological responses by GTPase activating proteins. *Physiol Rev* 92: 237-272.
14. Csepanyi-Komi, R., D. Safar, V. Grosz, Z. L. Tarjan, and E. Ligeti. 2013. In silico tissue-distribution of human Rho family GTPase activating proteins. *Small GTPases* 4: 90-101.
15. Kunisaki, Y., A. Nishikimi, Y. Tanaka, R. Takii, M. Noda, A. Inayoshi, K. Watanabe, F. Sanematsu, T. Sasazuki, T. Sasaki, and Y. Fukui. 2006. DOCK2 is a Rac activator that regulates motility and polarity during neutrophil chemotaxis. *J Cell Biol* 174: 647-652.
16. Lawson, C. D., S. Donald, K. E. Anderson, D. T. Patton, and H. C. Welch. 2011. P-Rex1 and Vav1 cooperate in the regulation of formyl-methionyl-leucyl-phenylalanine-dependent neutrophil responses. *J Immunol* 186: 1467-1476.
17. Gakidis, M. A., X. Cullere, T. Olson, J. L. Wilsbacher, B. Zhang, S. L. Moores, K. Ley, W. Swat, T. Mayadas, and J. S. Brugge. 2004. Vav GEFs are required for beta2 integrin-dependent functions of neutrophils. *J Cell Biol* 166: 273-282.
18. Costa, C., G. Germena, E. L. Martin-Conte, I. Molineris, E. Bosco, S. Marengo, O. Azzolino, F. Altruda, V. M. Ranieri, and E. Hirsch. 2011. The RacGAP ArhGAP15 is a master negative regulator of neutrophil functions. *Blood* 118: 1099-1108.
19. Cho, Y. J., J. M. Cunnick, S. J. Yi, V. Kaartinen, J. Groffen, and N. Heisterkamp. 2007. Abr and Bcr, two homologous Rac GTPase-activating proteins, control multiple cellular functions of murine macrophages. *Mol Cell Biol* 27: 899-911.
20. Gambardella, L., K. E. Anderson, C. Nussbaum, A. Segonds-Pichon, T. Margarido, L. Norton, T. Ludwig, M. Sperandio, P. T. Hawkins, L. Stephens, and S. Vermeren. 2011. The GTPase-activating protein ARAP3 regulates chemotaxis and adhesion-dependent processes in neutrophils. *Blood* 118: 1087-1098.
21. Csepanyi-Komi, R., G. Sirokmany, M. Geiszt, and E. Ligeti. 2012. ARHGAP25, a novel Rac GTPase-activating protein, regulates phagocytosis in human neutrophilic granulocytes. *Blood* 119: 573-582.

22. Lorincz, A. M., G. Szarvas, S. M. Smith, and E. Ligeti. 2014. Role of Rac GTPase activating proteins in regulation of NADPH oxidase in human neutrophils. *Free Radic Biol Med* 68: 65-71.
23. Testa, G., J. Schaft, F. van der Hoeven, S. Glaser, K. Anastassiadis, Y. Zhang, T. Hermann, W. Stremmel, and A. F. Stewart. 2004. A reliable lacZ expression reporter cassette for multipurpose, knockout-first alleles. *Genesis* 38: 151-158.
24. Nemeth, T., K. Futosi, C. Hably, M. R. Brouns, S. M. Jakob, M. Kovacs, Z. Kertesz, B. Walzog, J. Settleman, and A. Mocsai. 2010. Neutrophil functions and autoimmune arthritis in the absence of p190RhoGAP: generation and analysis of a novel null mutation in mice. *J Immunol* 185: 3064-3075.
25. Kovacs, M., T. Nemeth, Z. Jakus, C. Sitaru, E. Simon, K. Futosi, B. Botz, Z. Helyes, C. A. Lowell, and A. Mocsai. 2014. The Src family kinases Hck, Fgr, and Lyn are critical for the generation of the in vivo inflammatory environment without a direct role in leukocyte recruitment. *J Exp Med* 211: 1993-2011.
26. Frommhold, D., A. Ludwig, M. G. Bixel, A. Zarbock, I. Babushkina, M. Weissinger, S. Cauwenberghs, L. G. Ellies, J. D. Marth, A. G. Beck-Sickinger, M. Sixt, B. Lange-Sperandio, A. Zernecke, E. Brandt, C. Weber, D. Vestweber, K. Ley, and M. Sperandio. 2008. Sialyltransferase ST3Gal-IV controls CXCR2-mediated firm leukocyte arrest during inflammation. *J Exp Med* 205: 1435-1446.
27. Schindelin, J., I. Arganda-Carreras, E. Frise, V. Kaynig, M. Longair, T. Pietzsch, S. Preibisch, C. Rueden, S. Saalfeld, B. Schmid, J. Y. Tinevez, D. J. White, V. Hartenstein, K. Eliceiri, P. Tomancak, and A. Cardona. 2012. Fiji: an open-source platform for biological-image analysis. *Nat Methods* 9: 676-682.
28. Sperandio, M., J. Pickard, S. Unnikrishnan, S. T. Acton, and K. Ley. 2006. Analysis of leukocyte rolling in vivo and in vitro. *Methods Enzymol* 416: 346-371.
29. Mocsai, A., M. Zhou, F. Meng, V. L. Tybulewicz, and C. A. Lowell. 2002. Syk is required for integrin signaling in neutrophils. *Immunity* 16: 547-558.
30. Mocsai, A., E. Ligeti, C. A. Lowell, and G. Berton. 1999. Adhesion-dependent degranulation of neutrophils requires the Src family kinases Fgr and Hck. *J Immunol* 162: 1120-1126.
31. Ren, X. D., and M. A. Schwartz. 2000. Determination of GTP loading on Rho. *Methods Enzymol* 325: 264-272.
32. Benard, V., and G. M. Bokoch. 2002. Assay of Cdc42, Rac, and Rho GTPase activation by affinity methods. *Methods Enzymol* 345: 349-359.
33. Levay, M., B. Bartos, and E. Ligeti. 2013. p190RhoGAP has cellular RacGAP activity regulated by a polybasic region. *Cell Signal* 25: 1388-1394.
34. Nishida, N., C. Xie, M. Shimaoka, Y. Cheng, T. Walz, and T. A. Springer. 2006. Activation of leukocyte beta2 integrins by conversion from bent to extended conformations. *Immunity* 25: 583-594.
35. Lammermann, T., and R. N. Germain. 2014. The multiple faces of leukocyte interstitial migration. *Semin Immunopathol* 36: 227-251.
36. Park, H., M. M. Chan, and B. M. Iritani. 2010. Hem-1: putting the "WAVE" into actin polymerization during an immune response. *FEBS Lett* 584: 4923-4932.
37. Herter, J. M., J. Rossaint, H. Block, H. Welch, and A. Zarbock. 2013. Integrin activation by P-Rex1 is required for selectin-mediated slow leukocyte rolling and intravascular crawling. *Blood* 121: 2301-2310.
38. Watanabe, M., M. Terasawa, K. Miyano, T. Yanagihara, T. Uruno, F. Sanematsu, A. Nishikimi, J. F. Cote, H. Sumimoto, and Y. Fukui. 2014. DOCK2 and DOCK5 act additively in neutrophils to regulate chemotaxis, superoxide production, and extracellular trap formation. *J Immunol* 193: 5660-5667.
39. Wojciak-Stothard, B., A. Entwistle, R. Garg, and A. J. Ridley. 1998. Regulation of TNF-alpha-induced reorganization of the actin cytoskeleton and cell-cell junctions by Rho, Rac, and Cdc42 in human endothelial cells. *J Cell Physiol* 176: 150-165.

40. Elbim, C., S. Chollet-Martin, S. Bailly, J. Hakim, and M. A. Gougerot-Pocidalo. 1993. Priming of polymorphonuclear neutrophils by tumor necrosis factor alpha in whole blood: identification of two polymorphonuclear neutrophil subpopulations in response to formyl-peptides. *Blood* 82: 633-640.
41. Elbim, C., S. Bailly, S. Chollet-Martin, J. Hakim, and M. A. Gougerot-Pocidalo. 1994. Differential priming effects of proinflammatory cytokines on human neutrophil oxidative burst in response to bacterial N-formyl peptides. *Infect Immun* 62: 2195-2201.
42. Jablonska, E., M. Kiluk, W. Markiewicz, and J. Jablonski. 2002. Priming effects of GM-CSF, IFN-gamma and TNF-alpha on human neutrophil inflammatory cytokine production. *Melanoma Res* 12: 123-128.
43. Bouaouina, M., E. Blouin, L. Halbwachs-Mecarelli, P. Lesavre, and P. Rieu. 2004. TNF-induced beta2 integrin activation involves Src kinases and a redox-regulated activation of p38 MAPK. *J Immunol* 173: 1313-1320.
44. Schlam, D., R. D. Bagshaw, S. A. Freeman, R. F. Collins, T. Pawson, G. D. Fairn, and S. Grinstein. 2015. Phosphoinositide 3-kinase enables phagocytosis of large particles by terminating actin assembly through Rac/Cdc42 GTPase-activating proteins. *Nat Commun* 6: 8623.
45. Wang, L. D., S. B. Ficarro, J. N. Hutchinson, R. Csepanyi-Komi, P. T. Nguyen, E. Wisniewski, J. Sullivan, O. Hofmann, E. Ligeti, J. A. Marto, and A. J. Wagers. 2016. Phosphoproteomic profiling of mouse primary hematopoietic stem and progenitor cells reveals new regulators of HSPC mobilization. *Blood*.

Footnotes: 1 Experimental work was financially supported by the Hungarian Research Fund (OTKA K108382) to E.L., by the European Community's Seventh Framework Programme [FP7] under grant agreement n°HEALTH-F4-2011-282095 to M.S. and by Deutsche Forschungsgemeinschaft SFB914, project B1 to M.S.

551 **Figure legends**

552

553 **Fig.1. Measurement of leukocyte rolling and crawling in TNFα-stimulated mouse**
554 **cremaster muscle venules.** Intravital microscopy was conducted to investigate leukocyte
555 recruitment in the mouse cremaster muscle 2 hours after injection of rmTNFα (500 ng/mouse
556 intrascrotally). (A) Leukocyte rolling flux fraction (%) is presented as mean+SEM of 33
557 vessels from 10 wild type mice and 42 vessels of 12 *Arhgap25*$^{-/-}$ mice. Mean rolling velocity
558 of leukocytes (µm/s) (B) was quantified and is shown as bar chart (mean+SEM of 166
559 *Arhgap25*$^{+/+}$ cells and 190 *Arhgap25*$^{-/-}$ cells), ***: $P< .001$ compared to *Arhgap25*$^{+/+}$. (C)
560 Number of adherent cells per mm^2 vessel wall is given as mean+SEM of 10 (*Arhgap25*$^{+/+}$)
561 and 12 (*Arhgap25*$^{-/-}$) separate experiments. (D, E) Leukocyte crawling paths of individual
562 leukocytes of *Arhgap25*$^{+/+}$ (n=163 cells) and *Arhgap25*$^{-/-}$ (n=154 cells) mice. Direction of
563 blood flow is indicated by arrows. (F) Accumulated distance of leukocytes. Mean+ SEM of 8
564 wild type and 7 *Arhgap25*$^{-/-}$ mice. (G) Mean crawling velocity presented as mean+SEM of
565 163 *Arhgap25*$^{+/+}$ and 154 *Arhgap25*$^{-/-}$ cells. **: $P< .01$ compared to *Arhgap25*$^{+/+}$. (H)
566 Euclidean distance determines the length of section between starting and end points of
567 crawling pathways. Mean+SEM of 8 (*Arhgap25*$^{+/+}$) and 7 (*Arhgap25*$^{-/-}$) separate experiments
568 are shown.*: $P< .05$ compared to *Arhgap25*$^{+/+}$.

569

570 **Fig. 2. Transmigration of leukocytes under *in vivo* conditions.** (A-D) Representative
571 images of Giemsa-stained cremaster muscle whole mounts from *Arhgap25*$^{+/+}$ and *Arhgap25*$^{-/-}$
572 mice 3 hours after 500 ng intrascrotal rmTNFα injection. Images were captured with a Leica
573 DMI 6000 B microscope equipped with a 10x/0.30 NA dry objective (Leica) and a Leica DFC
574 480 camera. ROIs with high leukocyte infiltration (rectangles) are captured with 40x objective
575 and shown in the right side of the panel (B,D). Bars represent 100 µm. (E) Quantification of

576 total number of extravasated cells per mm^2 microvessel wall surface. (F) Distribution of
577 extravasated cell types (PMN: neutrophilic granulocytes, Eos: eosinophilic granulocytes,
578 Others: lymphocytes, macrophages and basophilic granulocytes). Mean+SEM of 3
579 (*Arhgap25*$^{+/+}$) and 7 (*Arhgap25*$^{-/-}$) separate experiments.***: *P*< .001 compared to
580 *Arhgap25*$^{+/+}$.
581
582 **Fig. 3. TNFα-induced leukocyte infiltration into the peritoneal cavity.**
583 (A) Hematoxylin and eosin staining of peritoneal tissues 3 hours after intraperitoneal injection
584 of TNFα. Left side of the panel indicates 2 representative images from *Arhgap25*$^{+/+}$ and 2
585 from *Arhgap25*$^{-/-}$ mice captured with a 10x objective. ROIs with high leukocyte infiltration
586 (rectangles) are captured with 40x objective and shown in the right side of the panel. Bars
587 represents 50 µm. Results shown are representatives of multiple experiments and of multiple
588 sections and fields. (B) Ly-6G^{+} cell count measured from peritoneal lavage of *Arhgap25*$^{+/+}$
589 and *Arhgap25*$^{-/-}$ mice 3 hours after TNFα administration. Data represent mean+SEM of 6
590 separate experiments. *: P< .05 compared to *Arhgap25*$^{+/+}$.
591
592 **Fig. 4. Leukocyte rolling and adhesion under flow conditions and transmigration in a**
593 **Transwell assay.** (A-C) *Ex vivo* flow chamber assay. Blood cells of *Arhgap25*$^{+/+}$ and
594 *Arhgap25*$^{-/-}$ mice were perfused through glass capillaries coated with different cell surface
595 molecules as indicated in panel B. Number of rolling (A) and adherent (B) leukocytes per
596 field of view (FOV) and mean rolling velocity (C) of wild type and *Arhgap25*$^{-/-}$ animals are
597 shown. Rolling was assessed in E-selectin coated chambers (A). E: rmE-selectin; I: rmICAM-
598 1; CXCL1: rmKC/CXCL1. Mean+SEM of 4 separate experiments. *: *P*< .05, **: *P*< .01, ***:
599 *P*<.001 compared to *Arhgap25*$^{+/+}$. (D) *In vitro* transmigration of *Arhgap25*$^{+/+}$ and *Arhgap25*$^{-/-}$
600 bone marrow neutrophils pretreated with TNFα toward CXCL12 in an FBS-coated Transwell

system. Data represent mean+SEM of 4 independent experiments. *: P< .05 compared to *Arhgap25*$^{+/+}$.

Fig. 5. Leukocyte transmigration in bone marrow chimeric mice carrying *Arhgap25*$^{-/-}$ or *Arhgap25*$^{+/+}$ hematopoietic cells. (A-D) Representative images of a Giemsa-stained cremaster muscle whole mount. Microscopic analysis was performed 3 hours after 500 ng intrascrotal rmTNFα injection. Images were captured with a Leica DMI 6000 B microscope equipped with a 10x/0.30 NA dry objective (Leica) and a Leica DFC 480 camera. ROIs with high leukocyte infiltration (rectangles) are captured with 40x objective and shown in the right side of the panel (B,D). Bars represent 100 µm. (E) Quantification of total number of extravasated cells per mm^2 microvessel wall surface. (F) Distribution of transmigrated cell types (PMN: neutrophilic granulocytes, Eos: eosinophilic granulocytes, Others: lymphocytes, macrophages, basophilic granulocytes). Mean+SEM of 3 separate experiments. *: *P*< .05 compared to *Arhgap25*$^{+/+}$.

Fig. 6. Investigation of the potential mechanism of altered migration in *Arhgap25*$^{-/-}$cells. (A) Cell surface expression of molecules relevant in leukocyte-endothelial cell interactions during recruitment. Mean fluorescence intensity relative to isotype control is presented. Mean+SEM of 5 separate experiments. Panel B shows binding of ICAM-1 to LFA1. Bone marrow-derived neutrophils were co-incubated with fluorescently labeled rmICAM-1. Bound ICAM-1 was detected with flow cytometry. Data are presented as mean fluorescence intensity ratio relative to unstimulated cells. CCXL1: rmKC/CXCL1, PMA: Phorbol 12-myristate 13-acetate. Mean+SEM of 4 separate experiments is shown. *: *P*< .05, **: *P*< .01. (C) GTP-bound active Rac amount in resting and stimulated bone marrow-derived neutrophils. Stimulation was carried out with 50 ng/mL TNFα in HBSS$^+$ medium at 37 °C for 10 min.

626 After lysis, active Rac was pulled down with PBD-GST-glutathione-sepharose beads. Bar
627 chart presents densitometric analysis of 6 (unstimulated) and 3 (TNFα-treated) separate
628 western blot experiments. Under the graph, a representative western blot experiment is shown.
629 Active and total Rac were decorated with anti-Rac antibody in 1:1000 dilution. (D, E)
630 Filamentous actin amount of bone marrow-derived neutrophils. Actin was stained with Alexa-
631 488-Phalloidin in 1:500 dilution and measured with flow cytometry. Pane D shows F-actin
632 content in resting neutrophils from *Arhgap25*$^{-/-}$ mice as mean fluorescence intensity of
633 phalloidin relative to *Arhgap25*$^{+/+}$. Mean+SEM of 4 separate experiments is present. **: $P<$
634 .01 compared to *Arhgap25*$^{+/+}$. (E) Changes in relative F-actin content of neutrophils treated
635 for 5, 10 and 15 minutes with 50 ng/mL TNFα. Mean fluorescence intensity of phalloidin is
636 expressed relative to unstimulated (0 min) control in each genotype. Mean±SEM of 6 separate
637 experiments is shown. *: $P<$ .05 compared to *Arhgap25*$^{+/+}$.

Figure1.

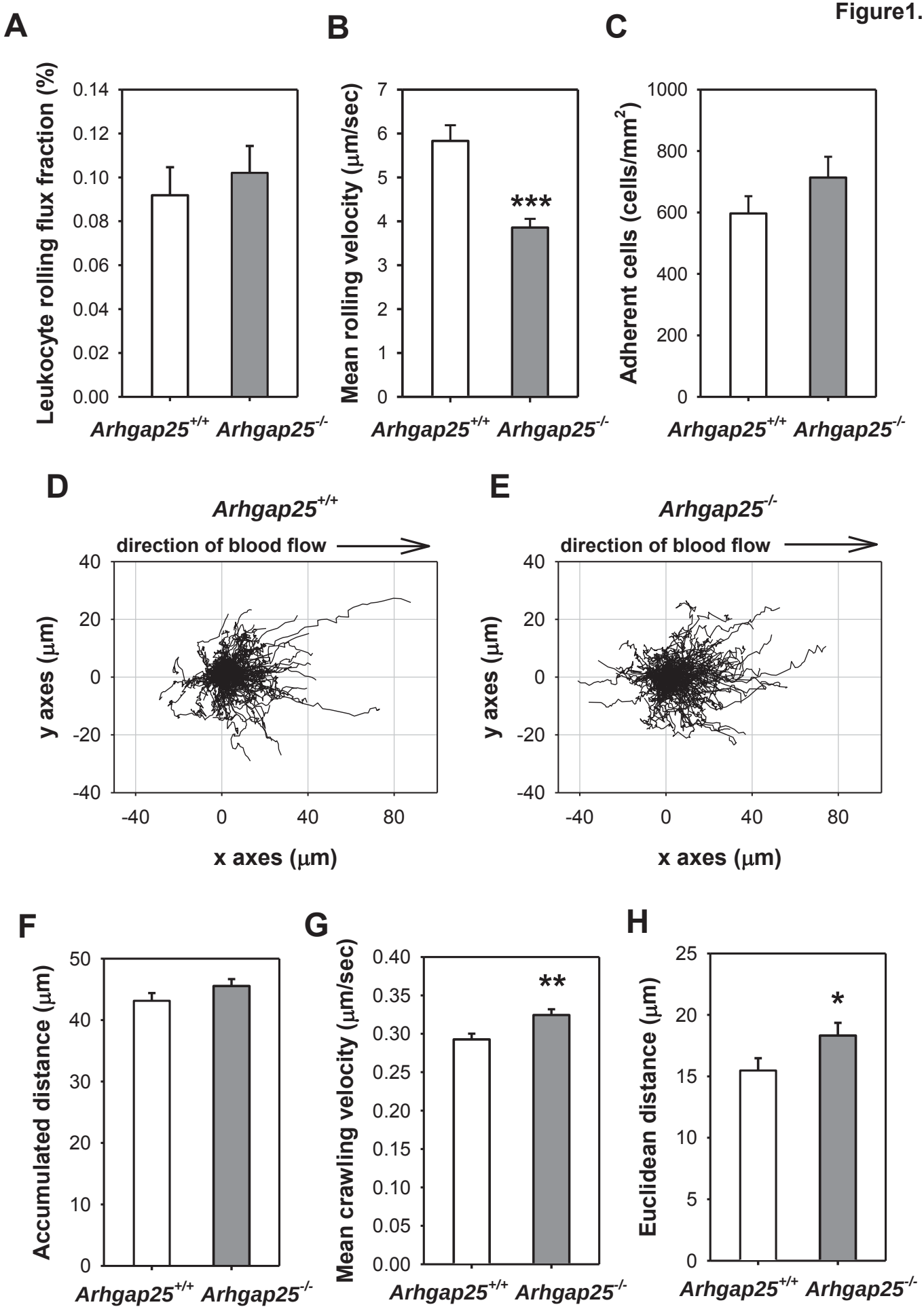
A
B
C
Leukocyte rolling flux fraction (%)
0.14
0.12
0.10
0.08
0.06
0.04
0.02
0.00
Arhgap25+/+ Arhgap25-/-
Mean rolling velocity (μm/sec)
7
6
5
4
3
2
1
0
***
Arhgap25+/+ Arhgap25-/-
Adherent cells (cells/mm2)
1000
800
600
400
200
0
Arhgap25+/+ Arhgap25-/-
D
Arhgap25+/+
direction of blood flow
y axes (μm)
40
20
0
-20
-40
-40
0
40
80
x axes (μm)
E
Arhgap25-/-
direction of blood flow
y axes (μm)
40
20
0
-20
-40
-40
0
40
80
x axes (μm)
F
Accumulated distance (μm)
50
40
30
20
10
0
Arhgap25+/+ Arhgap25-/-
G
Mean crawling velocity (μm/sec)
0.40
0.35
0.30
0.25
0.20
0.15
0.10
0.05
0.00
**
Arhgap25+/+ Arhgap25-/-
H
Euclidean distance (μm)
25
20
15
10
5
0
*
Arhgap25+/+ Arhgap25-/-

Figure 2.

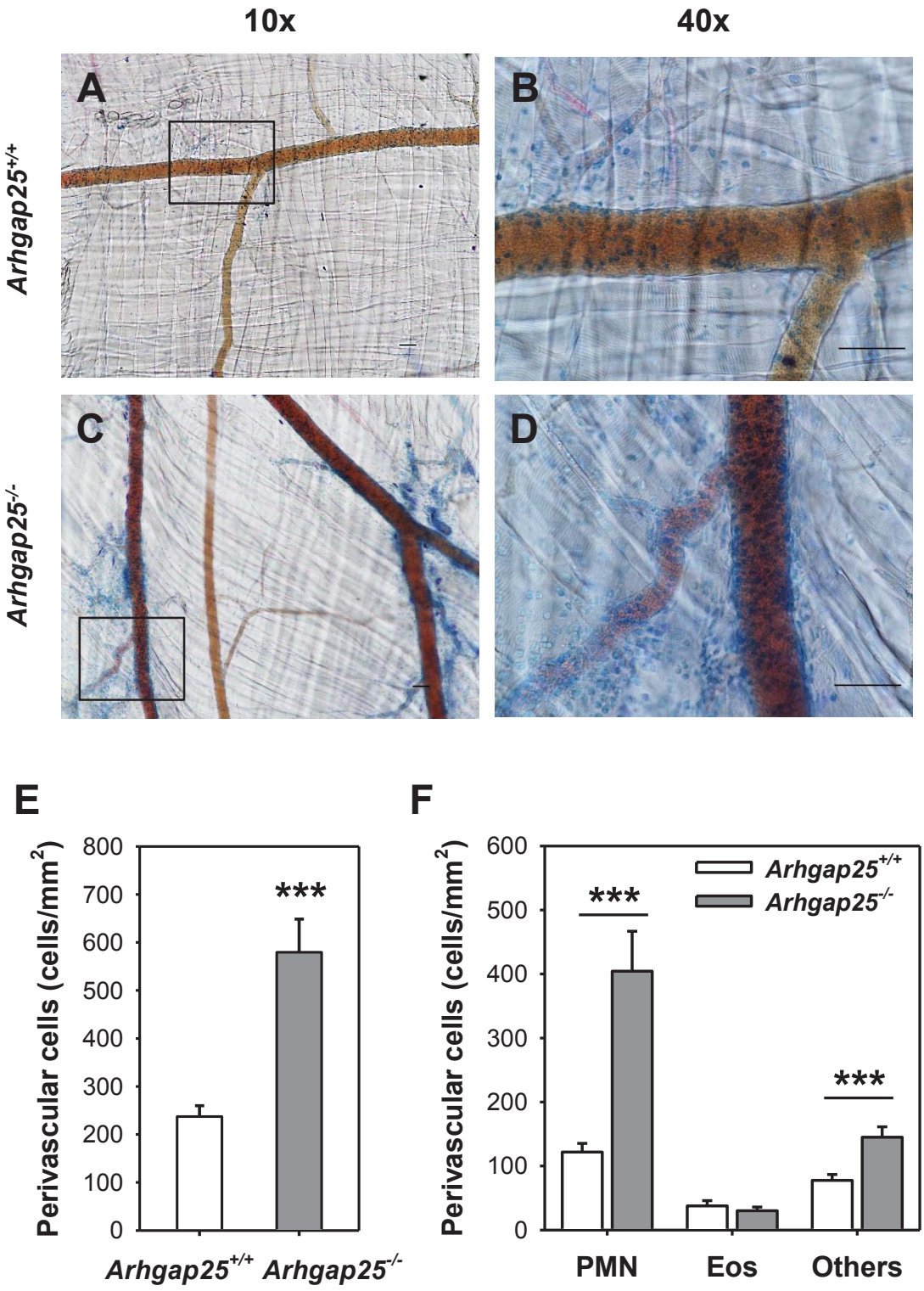
10x
40x
A
B
C
D
Arhgap25+/+
Arhgap25-/-
E
Perivascular cells (cells/mm2)
800
700
600
500
400
300
200
100
0
***
Arhgap25+/+
Arhgap25-/-
F
Perivascular cells (cells/mm2)
600
500
400
300
200
100
0
***
***
Arhgap25+/+
Arhgap25-/-
PMN
Eos
Others

Figure 3.

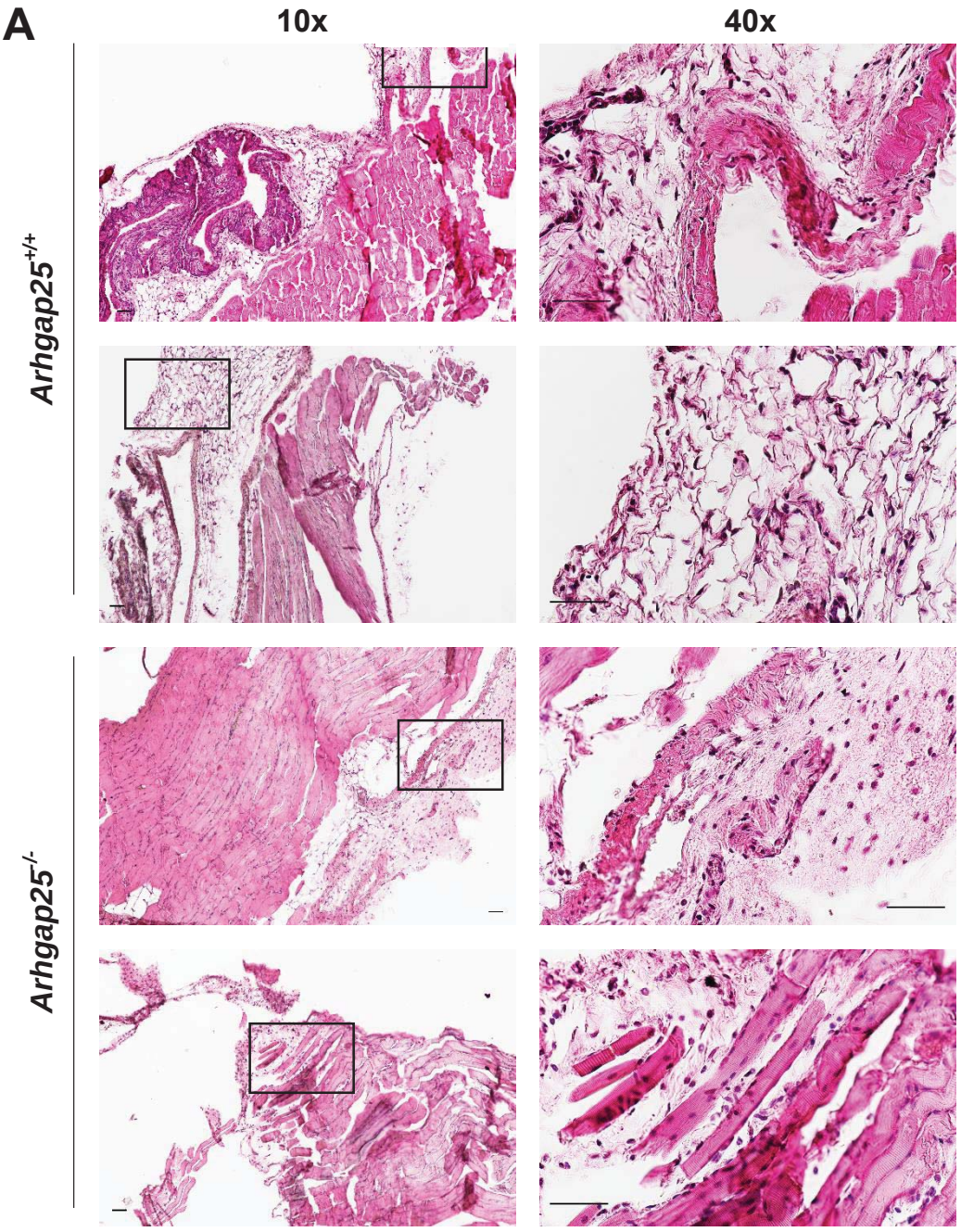
A
10x
40x
Arhgap25+/+
Arhgap25-/-

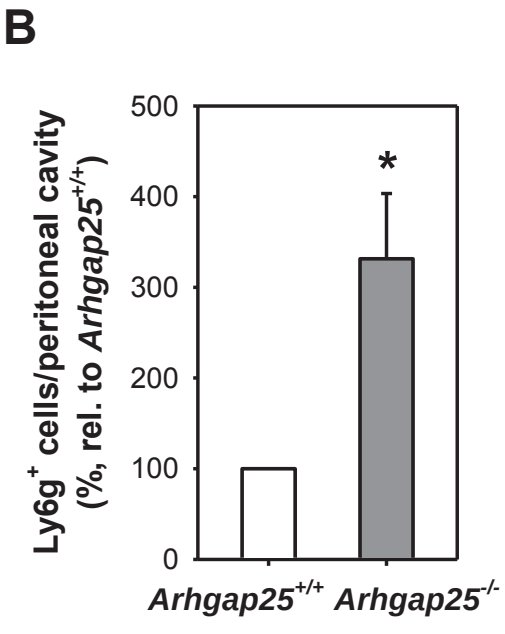
B
Ly6g+ cells/peritoneal cavity
(%, rel. to Arhgap25+/+)
500
400
300
200
100
0
*
Arhgap25+/+
Arhgap25-/-

Figure 4.

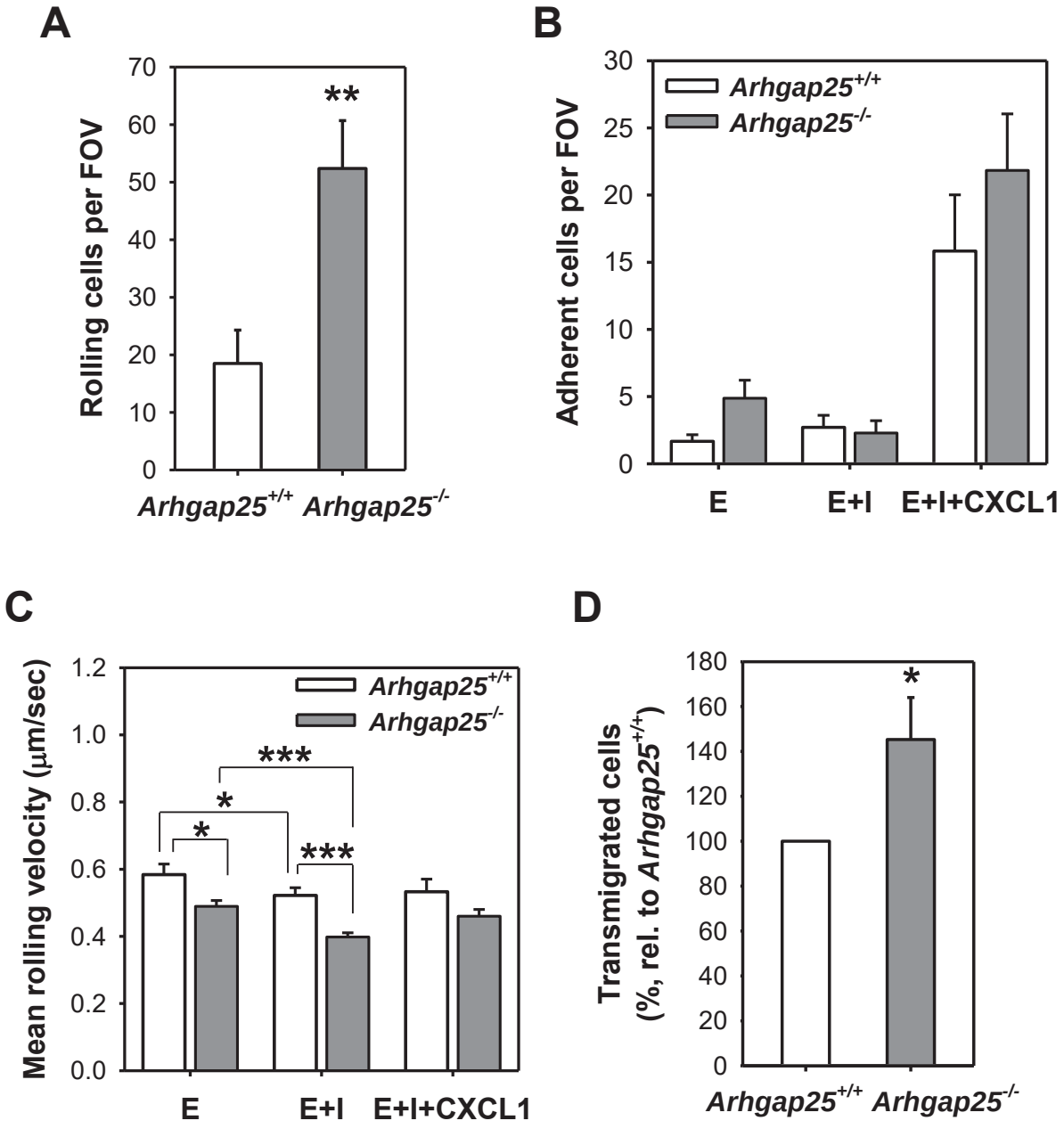
A
Rolling cells per FOV
70
60
50
40
30
20
10
0
**
Arhgap25+/+
Arhgap25-/-
B
Adherent cells per FOV
30
25
20
15
10
5
0
Arhgap25+/+
Arhgap25-/-
E
E+I
E+I+CXCL1
C
Mean rolling velocity (μm/sec)
1.2
1.0
0.8
0.6
0.4
0.2
0.0
Arhgap25+/+
Arhgap25-/-
***
*
*
***
E
E+I
E+I+CXCL1
D
Transmigrated cells
(%, rel. to Arhgap25+/+)
180
160
140
120
100
80
60
40
20
0
*
Arhgap25+/+
Arhgap25-/-

Figure 5.

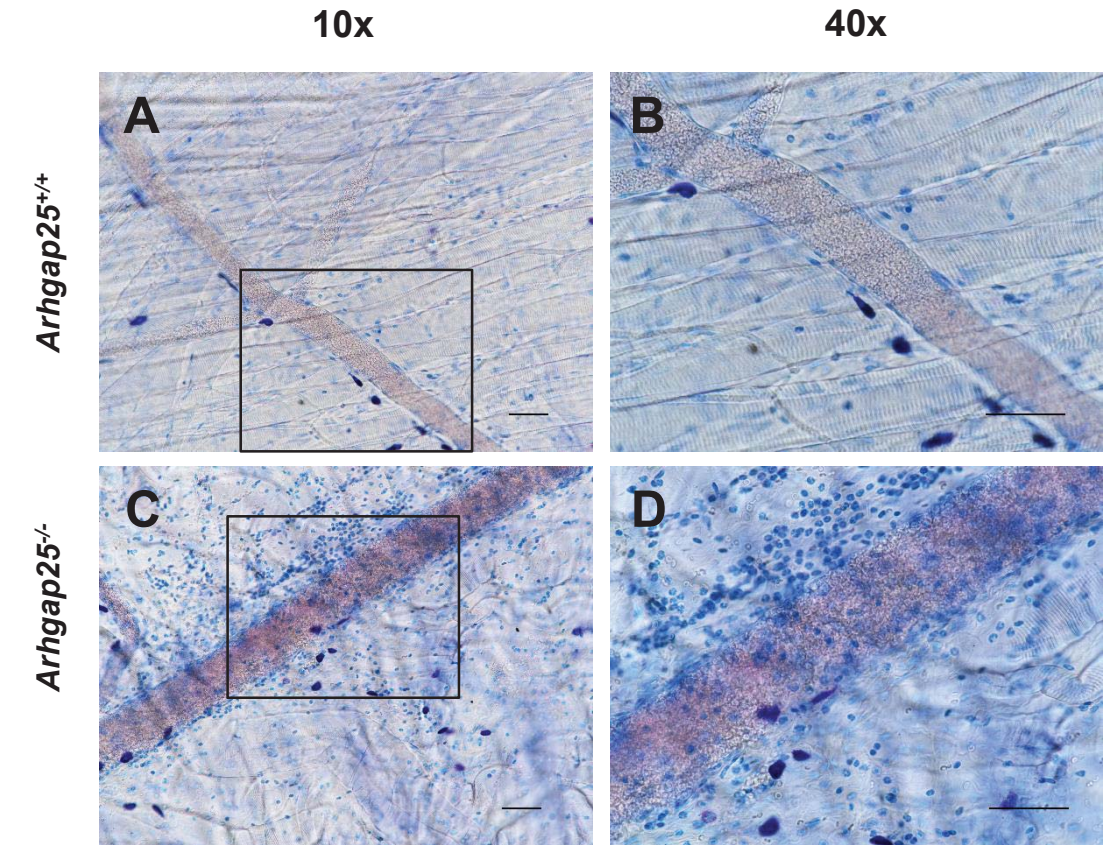
10x
40x
A
B
C
D
Arhgap25+/+
Arhgap25-/-

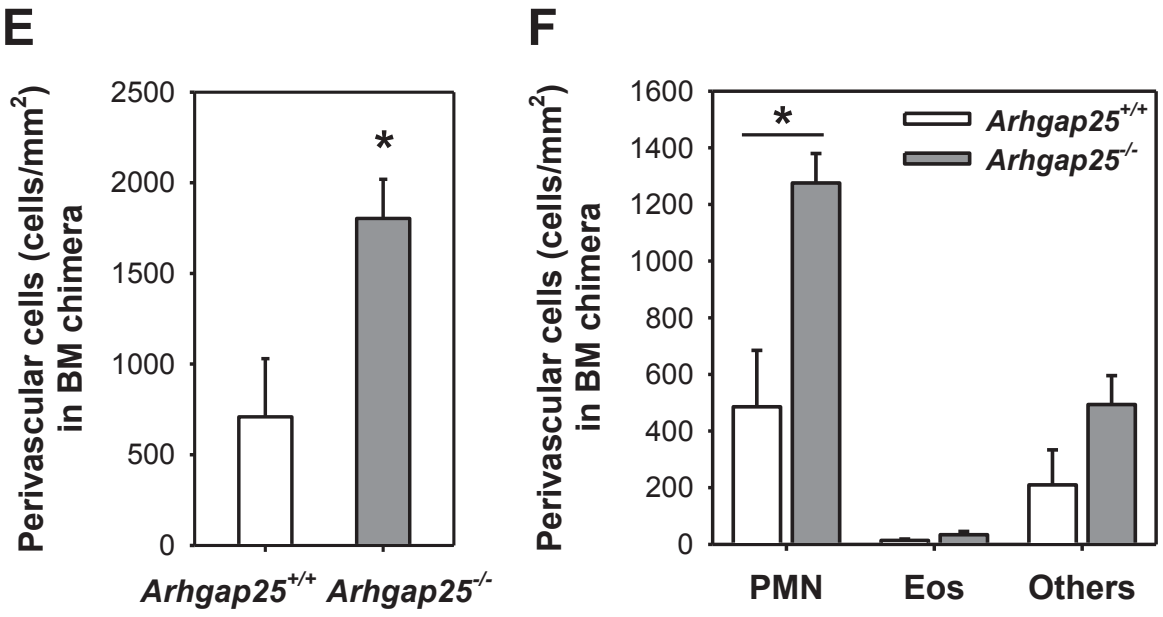
E
Perivascular cells (cells/mm2) in BM chimera
2500
2000
1500
1000
500
0
*
Arhgap25+/+
Arhgap25-/-
F
Perivascular cells (cells/mm2) in BM chimera
1600
1400
1200
1000
800
600
400
200
0
*
Arhgap25+/+
Arhgap25-/-
PMN
Eos
Others

Figure 6.

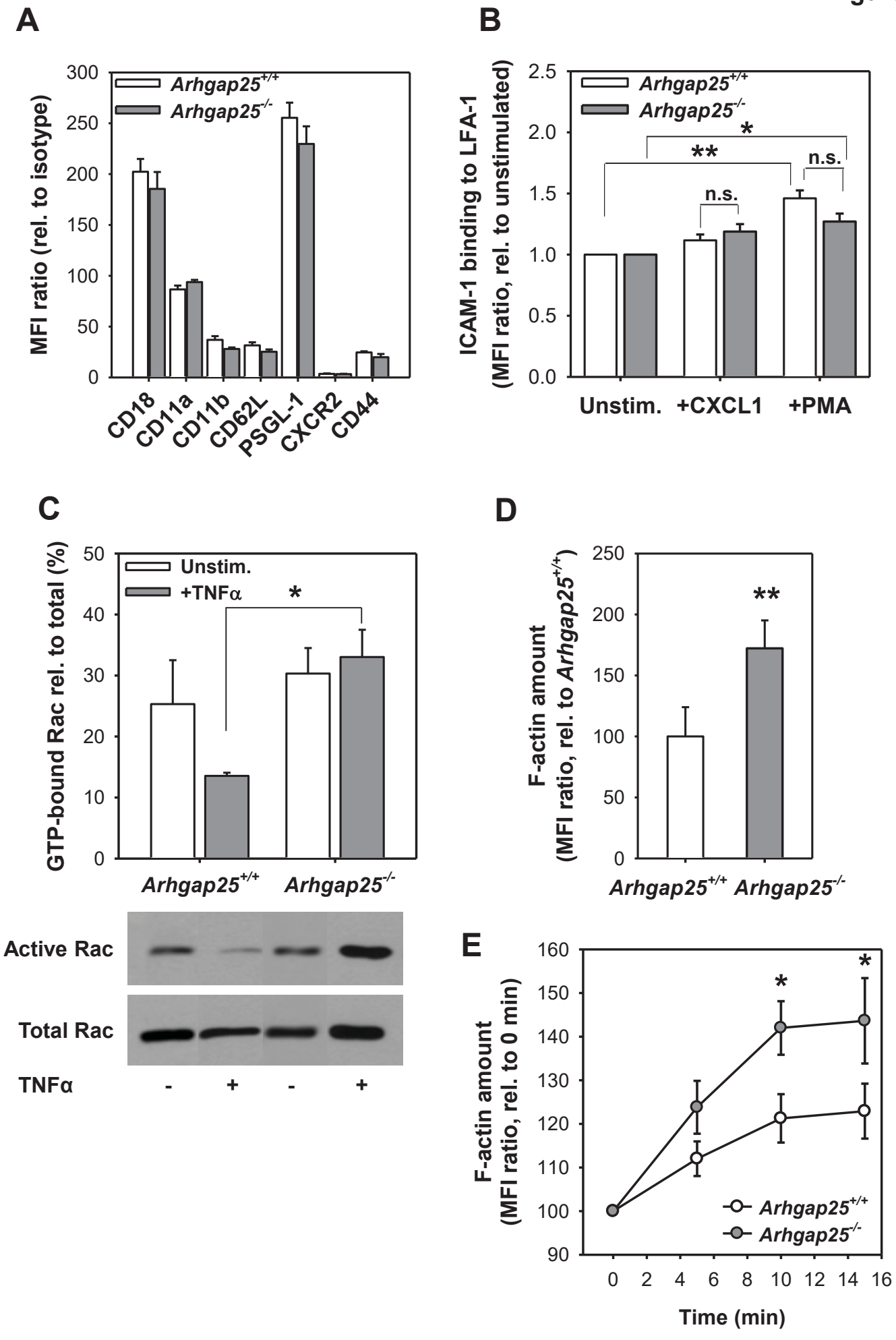
A
MFI ratio (rel. to isotype)
Arhgap25+/+
Arhgap25-/-
CD18
CD11a
CD11b
CD62L
PSGL-1
CXCR2
CD44
B
ICAM-1 binding to LFA-1 (MFI ratio, rel. to unstimulated)
n.s.
Unstim.
+CXCL1
+PMA
C
GTP-bound Rac rel. to total (%)
Unstim.
+TNFα
Active Rac
Total Rac
TNFα
D
F-actin amount (MFI ratio, rel. to Arhgap25+/+)
E
F-actin amount (MFI ratio, rel. to 0 min)
Time (min)

Table I. Blood parameters in *Arhgap25*$^{+/+}$ and *Arhgap25*$^{-/-}$ mice.

Parameter	*Arhgap25*$^{+/+}$	*Arhgap25*$^{-/-}$
Red blood cells, 10^6/uL	10.75 ± 0.08	10.69 ± 0.22
Hematocrit, %	52.78 ± 0.6	53.58 ± 1.57
MCH, pg	14.83 ± 0.06	14.55 ± 0.03
MCHC, g/dL	30.23 ± 0.14	29.05 ± 0.27
Reticulocytes, 10^3/μL	421.53 ± 32.01	469.35 ± 12.73
Platelets, 10^3/μL	807.00 ± 11.88	1017.25 ± 53.07
WBCs, 10^3/μL	5.72 ± 1.17	6.11 ± 0.59
Neutrophils, 10^3/μL	2.06 ± 0.27	2.32 ± 0.38
Lymphocytes, 10^3/μL	3.54 ± 1.20	3.60 ± 0.49
Monocytes, 10^3/μL	0.013 ± 0.005	0.085 ± 0.035
Eosinophils, 10^3/μL	0.103 ± 0.020	0.093 ± 0.011
Basophils, 10^3/μL	0.005 ± 0.003	0.008 ± 0.003

Data presented as mean ± SEM, n= 4 in each genotype. WBCs: white blood cells, MCH: mean corpuscular hemoglobin, MCHC: mean corpuscular hemoglobin concentration.